# Soliton formation and evolution in passively-mode-locked lasers with ultralong anomalous-dispersion fibers

Xueming Liu*

*State Key Laboratory of Transient Optics and Photonics, Xi'an Institute of Optics and Precision Mechanics, Chinese Academy of Sciences, Xi'an 710119, China*

(Received 16 May 2011; published 19 August 2011)

The soliton formation and evolution are numerically and experimentally investigated in passively-mode-locked lasers where pulses encounter ultralong anomalous-dispersion fibers. The pulse formation and evolution in lasers are determined by two balances, namely, nonlinearity and anomalous-dispersion balance and intracavity filtering and self-amplitude modulation balance. It is numerically found that a higher-energy soliton can be split into identical lower-energy multisolitons with exactly the same physical properties. Simulation results show that the separation of neighboring solitons is variational in the temporal domain. The temporal and spectral characteristics of solitons have large variations throughout the laser cavity, qualitatively distinct from the steady state of conventional solitons. The experimental observations confirm the theoretical predictions.

DOI: 10.1103/PhysRevA.84.023835 PACS number(s): 42.65.Tg, 42.81.Dp, 42.55.Wd, 42.65.Re

## I. INTRODUCTION

The formation and evolution of pulses in fibers are rich and fascinating subjects [1–5]. Fiber-based short-pulse sources attract extensive attention because they are compact and are cheap besides possessing high stability and low noise. Passively-mode-locked fiber lasers are able to easily generate self-starting short pulses so that they can be investigated extensively in principle and experiment [6–11]. When a fiber laser is made of fibers with purely anomalous group-velocity dispersion (GVD) or net-anomalous GVD, solitons with the hyperbolic-secant profile and spectral sidebands can be formed by the balance between the nonlinearity of the material and the anomalous GVD [1,12].

Conventional solitons are static and show chirp-free evolution within the laser cavity if the laser is composed of fibers with the uniform anomalous dispersion (an example is shown in Fig. 9 of Ref. [13]). Based on the master equation, the exact solution for the static soliton is given by $u(t) = A_0\mathrm{sech}(t/\tau)$ [14,15], where $\tau$ is the normalized pulse width. For the hyperbolic-secant-like solitons, an important requirement is that the nonlinear phase shift $\phi_{NL}$ per round trip must be very small [13,15]. Usually, it is limited by $\phi_{NL} = \frac{\omega}{c}\int_0^L n_2 I(z)dz \ll 2\pi$, where $\omega$, $c$, $I$, $L$, and $n_2$ are the angular frequency, speed of a light wave in vacuum, intensity, propagation distance, and nonlinear refractive index of the medium, respectively. As a result, the total length of the laser cavity for hyperbolic-secant-like solitons is as short as several meters to tens of meters.

However, when the cavity length of a fiber laser with anomalous GVD is as long as several hundred meters, what will happen? The current paper answers this question. In this paper, the pulse properties for a passively-mode-locked laser with an ultralong anomalous-dispersion fiber are investigated numerically and experimentally, including the dynamic evolution from noise to soliton, the enhancement of spectral sidebands with pumping strength, the multiple-soliton evolution and mechanism, and the intracavity evolution of solitons. For the nonlinear polarization rotation technique, self-amplitude modulation (SAM) can model the saturable absorber action due to polarization additive pulse mode locking (P-APM) [15]. Besides the nonlinearity and anomalous-GVD balance, the balance between the intracavity filtering and the SAM also play a key role in the soliton shaping.

## II. THEORETICAL MODEL

The master equation [1] and the complex Ginzburg-Landau equation [16,17] have been used widely to predict the pulse formation and evolution of passively-mode-locked lasers because they usually can offer the exact solutions for solitons. In this paper, the passive mode locking of a laser is based on the nonlinear polarization rotation evolution in which an ellipse is resolved into right- and left-hand circular polarization components of different intensities. The two coupled nonlinear Schrödinger equations (NLSEs) that involve a vector electric field can model the light-wave propagation in the weakly birefringent fibers more accurately.

When the total cavity length is several meters, the coupled NLSEs have to involve terms, such as the wave-number difference between the two modes and the four-wave mixing [18]. Contrarily, while the total cavity length $L$ (here, $L >$ 100 m) is far longer than the beat length $L_B$ of the fiber (usually $L_B \approx 1$ m), the coupled equations can ignore the terms related to the four-wave mixing [19,20]. Then, the coupled equations are expressed by [19]

$$\frac{\partial u}{\partial z} = -\frac{\alpha}{2}u - \delta\frac{\partial u}{\partial T} - i\frac{\beta_2}{2}\frac{\partial^2 u}{\partial T^2} + i\gamma\left(|u|^2 + \frac{2}{3}|v|^2\right)u + \frac{g}{2}u + \frac{g}{2\Omega_g^2}\frac{\partial^2 u}{\partial T^2},$$

$$\frac{\partial v}{\partial z} = -\frac{\alpha}{2}v + \delta\frac{\partial v}{\partial T} - i\frac{\beta_2}{2}\frac{\partial^2 v}{\partial T^2} + i\gamma\left(|v|^2 + \frac{2}{3}|u|^2\right)v + \frac{g}{2}v + \frac{g}{2\Omega_g^2}\frac{\partial^2 v}{\partial T^2}. \quad (1)$$

*liuxueming72@yahoo.com

 

Here, $u$ and $v$ are the envelopes of the optical pulses along the two orthogonal polarization axes of the fiber. $\alpha$, $\delta$, $\beta_2$, $\gamma$, and $\Omega_g$ are the loss coefficient of the fiber, the group-velocity difference between the two polarization modes, the fiber dispersion, the cubic refractive nonlinearity of the medium, and the bandwidth of the laser gain, respectively. The variables $T$ and $z$ represent the time and the propagation distance, respectively. $g$ is the net gain, which describes the gain function of the doped fiber. It is expressed by $g = g_0 \exp(-E_p/E_s)$ [21], where $g_0$, $E_s$, and $E_p$ are the small-signal gain, the gain saturation energy, and the pulse energy, respectively. $g_0$ is related to the doping concentration, and $E_s$ is dependent on pump power [22,23]. When the soliton propagates through the P-APM element, the intensity transmission $T_i$ is expressed as

$$T_i = \sin^2(\theta)\sin^2(\varphi) + \cos^2(\theta)\cos^2(\varphi) + 0.5\sin(2\theta)\sin(2\varphi)\cos(\phi_1 + \phi_2), \quad (2)$$

where $\phi_1$ is the phase delay caused by the polarization controllers and $\phi_2$ is the phase delay resulting from the fiber, which includes both the linear phase delay and the nonlinear phase delay. The polarizer and analyzer have an orientation of angles $\theta$ and $\varphi$ with respect to the fast axis of the fiber, respectively [19].

Equation (1) is solved with a predictor-corrector split-step Fourier method [24]. For the modeling, we use the following parameters for our simulations for possibly matching the experimental conditions: $\alpha = 0.2$ dB/km, $g_0 = 2$ m$^{-1}$, $\Omega_g =$ 30 nm, $\gamma = 4.5$ W$^{-1}$ km$^{-1}$, and $\beta_2 = 55$ ps$^2$/km for an erbium-doped fiber (EDF) and $\gamma = 1.3$ W$^{-1}$ km$^{-1}$ and $\beta_2 = -22$ ps$^2$/km for a single-mode fiber (SMF). The length of the EDF and SMF is 11 and 702 m, respectively. The above parameters are from the data sheets of fiber products.

## III. SIMULATION RESULTS

### A. Dynamic evolution from noise to soliton

To numerically simulate the feature and behavior of the proposed laser, the simulation starts from an arbitrary signal and converges into a stable solution with appropriate parameters after a finite number of traversals of the cavity. In this paper, a noise signal is initialized as shown in Fig. 1. Numerical simulations show that, for $\theta = \pi/3.5$, $\varphi = \pi/10$, $\phi_1 = 0.9 + \pi/2$, and $E_s = 0.025$ nJ, the pulse eventually converges toward a steady-state solution, and exactly the same stable solutions are reached from distinct initial noise fields. Figure 1 shows the transient temporal evolution from a noise signal to a stable pulse. From Fig. 1, it is seen that the soliton solution approaches the stability when the round-trip number $N_R$ is more than 70. The stable solution of a soliton is shown in the inset of Fig. 1. It is found that the pedestal of solitons has the oscillating structure, and the pulse duration and peak power are about 3.4 ps and 18 W, respectively, corresponding to the pulse energy of about 61 pJ.

The numerical results show that, when the pumping strength $E_s$ is lower than a certain value, the soliton quickly dies out. An example for $E_s = 0.004$ nJ is shown in Fig. 2. In simulation, a stable soliton solution, as shown in Fig. 1, is initialized for the first round-trip number $N_R = 1$. The other parameters are the same as in Fig. 1. From Fig. 2, we can see that the soliton quickly weakens and then disappears.

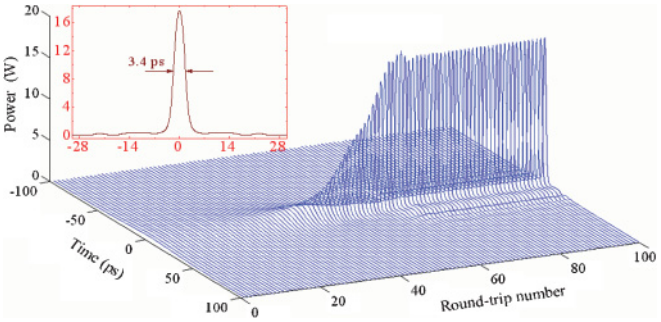


FIG. 1. (Color online) Pulse evolution from noise to soliton. The parameters used are $\theta = \pi/3.5$, $\varphi = \pi/10$, $\phi_1 = 0.9 + \pi/2$, and $E_s = 0.025$ nJ. A noise signal is initialized for the first round-trip number $N_R = 1$. Inset, the stationary soliton solution at the stable state.

### B. Enhancement of spectral sidebands with pumping strength

Numerical results show that there is no mode locking when the pumping strength $E_s$ is less than 0.01 nJ. From the experimental point of view, this corresponds to the case that the laser is operating below the mode-locking threshold. When $E_s$ is more than 0.012 nJ, the stable soliton solutions are obtained in simulations. Some examples for $E_s = 0.013$, 0.018, 0.022, 0.025, and 0.029 nJ are shown in Fig. 3. From Fig. 3(f), we can observe that the peak power of the solitons increases and the pulse duration narrows with the enhancement of $E_s$. The solitons are characterized by the appearance of the sidebands in the optical spectrum as shown in Figs. 3(a)–3(e). Once $E_s$ is fixed, a soliton with the fixed-peak power, pulse width, and spectral sidebands will be formed, which are independent of the initial conditions. From Fig. 3, it is found that, with the increase in $E_s$, more spectral sidebands are visible, and they become stronger and stronger, and the positions of the sidebands become closer to the peak of the soliton spectrum. The theoretical explanations are as follows. According to the

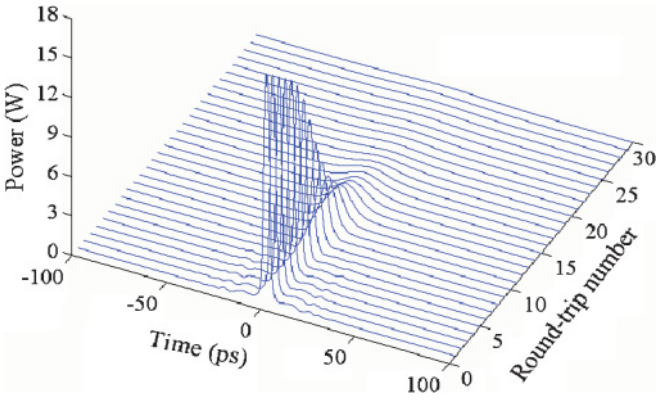


FIG. 2. (Color online) Annihilation evolution of a soliton. A stable soliton solution, as shown in Fig. 1, is initialized for the first round-trip number $N_R = 1$. Except for $E_s = 0.004$ nJ, the other parameters are the same as in Fig. 1.

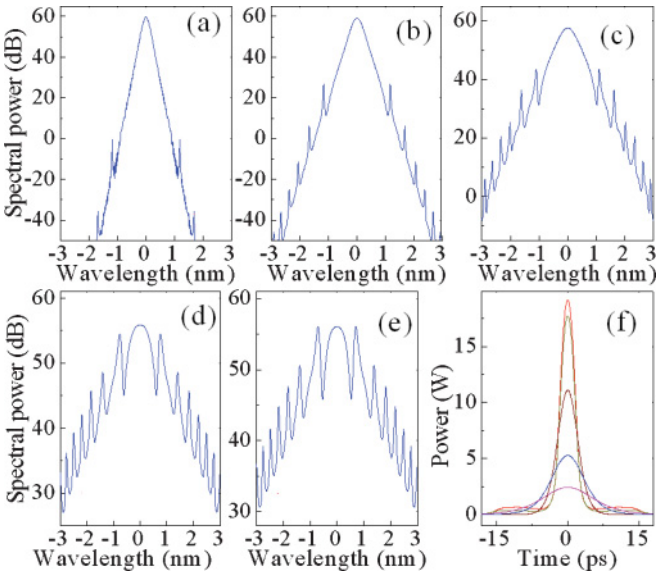


FIG. 3. (Color online) Spectral power profiles of solitons at the pumping strength (a) $E_s = 0.013$ nJ, (b) $E_s = 0.018$ nJ, (c) $E_s = 0.022$ nJ, (d) $E_s = 0.025$ nJ, and (e) $E_s = 0.029$ nJ. (f) Pulse profiles at $E_s = 0.013$, 0.018, 0.022, 0.025, and 0.029 nJ from bottom to top.

phase-matching conditions, the frequency offset $\Delta\omega$ from the peak of the soliton spectrum is given by [15,25]

$$\Delta\omega = \pm\frac{1}{\tau}\sqrt{m\frac{8Z_0}{Z_p} - 1}, \tag{3}$$

where $m$ is an integer, $\tau$ is the normalized pulse width, $Z_p$ is the perturbation length, and $Z_0$ is the soliton period that is expressed by

$$Z_0 = 0.5\pi\ \tau^2/|\beta_2|. \tag{4}$$

From Eqs. (3) and (4) and Fig. 3(f), one can see that the pulse width will decrease with respect to the increase in $E_s$, then $Z_0$ will decrease, and the sidebands will be located closer to the peak of the soliton.

### C. Multisoliton evolution and mechanism

When the pumping strength $E_s$ is enhanced, multiple solitons in the laser cavity are generated. Figure 4 shows the dynamic evolution from a soliton to two solitons when $E_s$ is enhanced from 0.025 to 0.055 nJ. Different from the bound

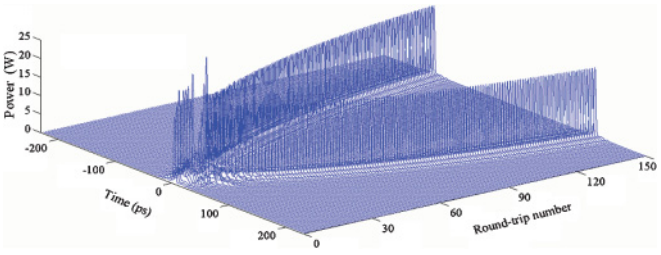


FIG. 4. (Color online) Dynamic evolution, showing the splitting process from a soliton to two solitons. Except for $E_s = 0.055$ nJ, the other parameters are the same as in Fig. 2.

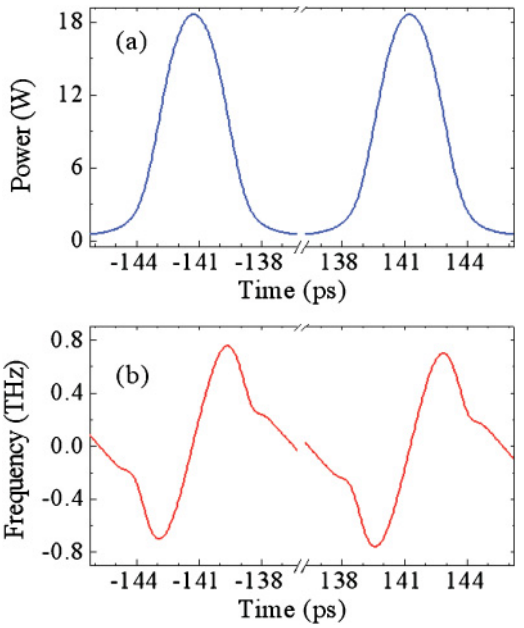


FIG. 5. (Color online) (a) Temporal power profile and (b) instantaneous frequency of two solitons at $E_s = 0.055$ nJ.

solitary pulses, where the peak separation of neighboring solitons is fixed or almost fixed [6,13], in this paper, the separation of two solitons is variational. From Fig. 4, it is clearly shown that the separation of two solitons is different at the different round trips. However, the two solitons have the same physical properties, such as the identical energy, width, and phase. An example for the detailed characteristics of the two solitons is demonstrated in Fig. 5.

Figure 5 shows the power profile and instantaneous frequency of two solitons at the round-trip number $N_R = 150$. It is clear that the two solitons have the same temporal power profile and instantaneous frequency. Therefore, our theoretical results confirm the experimental observations on the soliton energy quantization effect [11,18].

Figure 6 demonstrates the formation and evolution of a dual soliton from a noise signal at $E_s = 0.08$ nJ. All parameters are the same as in Fig. 1, except for $E_s$. Different from Fig. 1, where only a stable soliton is formed, Fig. 6 shows that one soliton is generated first from the noise signal, and successively, it is split into two solitons with the same physical characteristics. From Fig. 6, it is strange that the solitons are the periodic evolution with three processes of lower, middle, and higher peak power, in turn. This phenomenon is similar to the period tripling bifurcation reported in Ref. [16]. From Figs. 4 and 6, we can see that there is a chaos process before a soliton is split into two solitons.

If the pumping strength $E_s$ is further enhanced, three solitons with exactly the same pulse properties are generated. In simulations, except for $E_s = 0.096$ nJ, the other parameters are the same as in Fig. 6. The noise is shaped into one soliton, and then a soliton breaks up into two and three solitons, in turn. After three solitons are formed, they will interact in the evolution. From Fig. 7, one can observe that the separation of the neighboring solitons is changeable with respect to the round-trip number. The local soliton interaction mediated

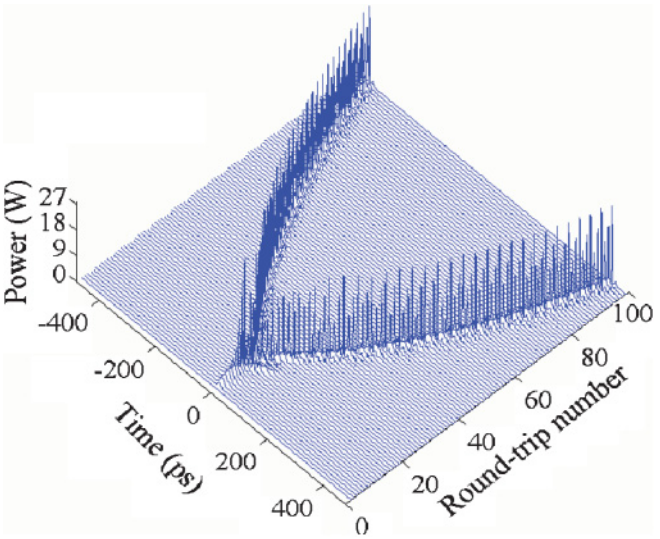


FIG. 6. (Color online) Dual-soliton formation and evolution from a noise. Except for $E_s = 0.08$ nJ, the other parameters are the same as in Fig. 1.

through the dispersive waves and the global soliton interaction caused by the continuous-wave (cw) components play the key roles for the repulsion and attraction of pulses [26]. From Figs. 1, 4, 6, and 7, we can observe that the soliton number in the laser oscillator increases with the enhancement of $E_s$. The numerical results are in agreement with the experimental observations.

There are two different mechanisms of multisoliton generation in lasers. One is the soliton shaping of the linear waves, and the other one is the pulse splitting [12,18]. Tang *et al*. proved that the soliton shaping of the dispersive waves or the cw components plays a key role in the generation of additional solitons when the laser-ring length is as short as several meters

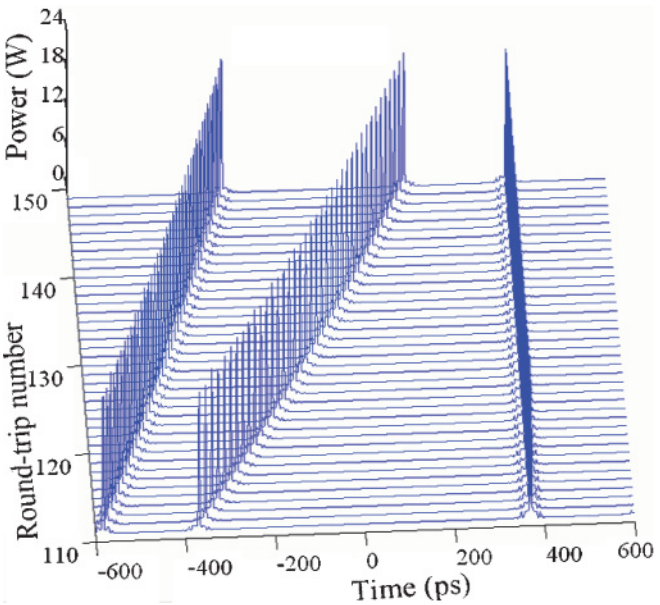


FIG. 7. (Color online) Evolution and interaction of three solitons at $E_s = 0.096$ nJ. Except for $E_s$, the other parameters are the same as in Fig. 6.

to tens of meters [18]. Note that, in this case, the coupled NLSEs have to involve the terms related to the wave-number difference and the four-wave mixing.

From Figs. 4–7, it is easily found that the mechanism of pulse splitting determines the multisoliton generation in the ultralong fiber lasers. The operation of pulse splitting is managed by the soliton energy quantization effect [11]. Obviously, here, the mechanism of soliton formation is different from the one in the paper of Tang *et al*. It originates from the fact that the coupled NLSEs skim the terms related to the wave-number difference and the four-wave mixing in the current paper.

### D. Intracavity evolution of solitons

Figures 8(a) and 8(b) show the intracavity pulse evolutions in the temporal domain and spectral domain at $E_s = 0.024$ nJ. The detailed pulse characteristics of one cavity round trip are illustrated in Fig. 9. The soliton propagates through the undoped fiber (from 0 to 700 m and from 711 to 713 m), the doped gain fiber (from 700 to 711 m), the output coupler (at 712 m), and the P-APM (at 713 m). Figures 9(a) and 9(b) show the intracavity pulse evolutions for the pulse duration, peak power, spectral peak, and slope of the instantaneous frequency at time $T = 0$, $S_{IF}$, over one cavity round trip, respectively. Figure 9(c) illustrates three examples for the instantaneous frequency of pulses before and after the EDF and at the intracavity position of 600 m.

From Figs. 8(a) and 8(b), one can observe that the variations in the temporal and spectral widths and their peaks during the intracavity propagation are very large, qualitatively distinct from the behavior in the typical soliton regime where there are

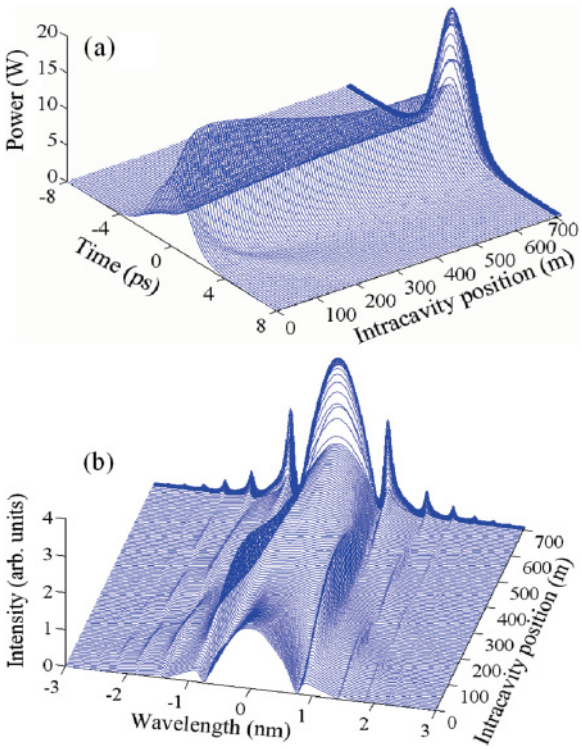


FIG. 8. (Color online) Intracavity pulse evolutions in (a) the temporal domain and (b) the spectral domain at $E_s = 0.024$ nJ.

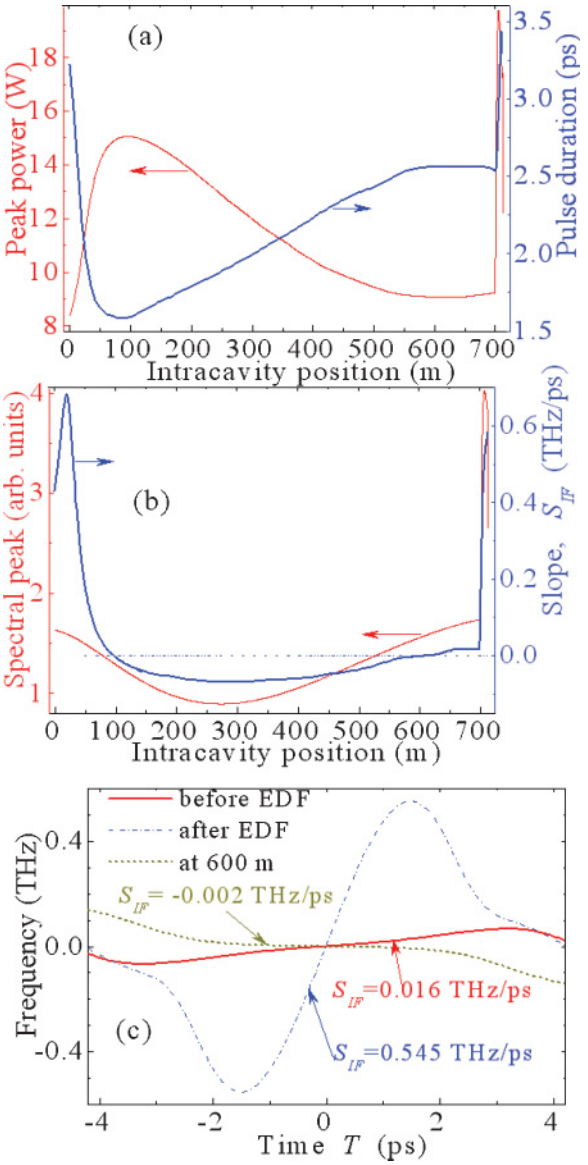


FIG. 9. (Color online) (a) Pulse duration and peak power and (b) spectral peak and slope of instantaneous frequency at $T = 0$, $S_{IF}$ along the intracavity position at $E_s = 0.024$ nJ. (c) Instantaneous frequency of pulses before and after the EDF and at the intracavity position of 600 m. Intracavity position, the undoped fiber (i.e., the SMF) from 0 to 700 m and from 711 to 713 m, the doped gain fiber (i.e., the EDF) from 700 to 711 m, the output coupler at 712 m, and the P-APM at 713 m.

little fluctuations and even the steady state [13]. Figure 8(b) shows that the linear dispersive waves are rapidly amplified when they pass through the EDF. Figures 9(a) and 9(b) exhibit that both the peak power of the pulses and the spectral peak quickly increase along the gain fiber. The instantaneous frequency of the pulses is markedly enhanced after the EDF [Fig. 9(c)] so that the chirp of the pulses is significantly accumulated via the gain fiber.

From Fig. 9(a), one can see that the pulse duration (or peak power) decreases (or increases) in the beginning of the SMF and then increases (or decreases) monotonically in the remaining SMF until a position of about 600 m. The pulse-breathing ratio in the SMF is more than 2, from 1.58 to 3.22 ps of pulse duration. When the pulses propagate through the SMF from about 600 to 700 m, they are almost in a steady evolution with the fixed pulse duration and peak power. Obviously, the pulse evolution of the proposed laser in the intracavity is very different from that of conventional soliton lasers, although both operate on the net-anomalous-dispersion regime.

Figures 9(b) and 9(c) show that the slope of instantaneous frequency at $T = 0$, $S_{IF}$, increases from 0.016 to 0.545 THz/ps when the pulses propagate through the gain fiber. In fact, $S_{IF}$ in most of the SMFs is limited from $-0.07$ to 0.02 THz/ps. By comparing to self-similar pulses whose $S_{IF}$ is over 7 THz/ps (Fig. 9 in Ref. [13]), obviously, $S_{IF}$ here decreases by more than 2 orders of magnitude. Especially, $S_{IF}$ is from $-0.002$ to 0.016 THz/ps at the cavity position of 600 to 700 m [Fig. 9(b)] so that solitons have a very low chirp at this range.

From Figs. 8(a) and 9(a), the proposed laser can be regarded as two different physical processes. The first process is similar to the stretched-pulse lasers where the pulse is compressed from 0 to ~100 m of the SMF, and successively, it is stretched from ~100 to ~600 m of the SMF. In this process, both the nonlinearity and the anomalous-GVD balance and the intracavity filtering and the SAM balance play the key roles and complete the soliton shaping. The second process is similar to the conventional soliton propagation within the fiber from ~600 to ~700 m. In the second process, only the balance of nonlinearity and anomalous-GVD contributes to the soliton evolution.

## IV. EXPERIMENTAL SETUP AND RESULTS

The schematic of the fiber laser that we used in the experiments is shown in Fig. 10. It contains a polarization-sensitive isolator, two sets of polarization controllers (PCs), a fused coupler with 30% output, a wavelength-division multiplexing coupler, a 11-m-long EDF with absorption 6 dB/m at 980 nm, a 700-m-long standard SMF, and some fiber pigtails. The EDF provides the gain amplification for the laser system pumped by a 977-nm laser diode. The parameters are the same as the numerical simulations. An autocorrelator, with the scan range of 1 ns, is used to measure the output pulses.

With the appropriate orientation and pressure settings of the two PCs, mode locking self-starts at a pump power of about

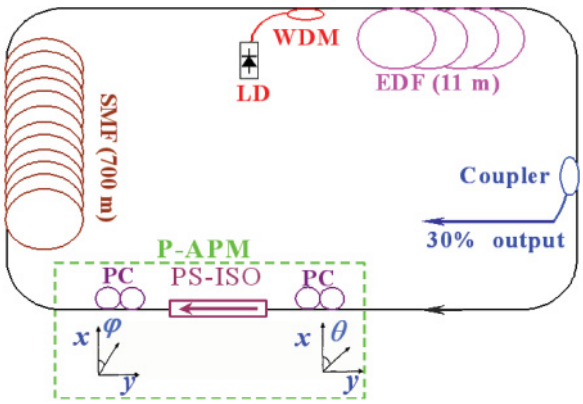


FIG. 10. (Color online) Schematic of the experimental setup for the proposed laser.

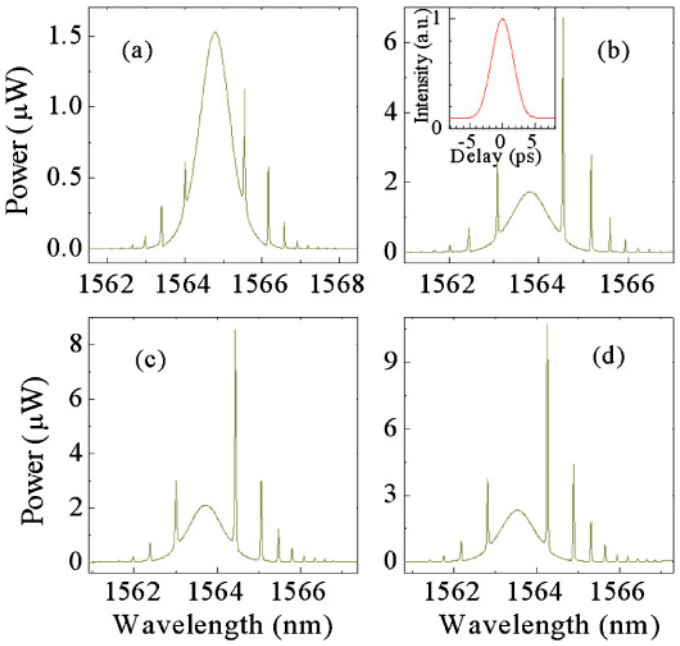


FIG. 11. (Color online) Experimental observations for the optical spectra of solitons at the pump power (a) $P = 18$ mW, (b) $P = 20$ mW, (c) $P = 23$ mW, and (d) $P = 26$ mW. Inset, the autocorrelation trace at $P = 20$ mW.

14 mW. Beyond the threshold power, the fiber laser delivers the typical solitons with the spectral sidebands. Figures 11(a)–11(d) show four examples at the pump power $P = 18$, 20, 23, and 26 mW, respectively, and the corresponding output power is about 0.8, 1, 1.3, and 1.6 mW. From Fig. 11, it is found that, with the increase in $P$, the spectral sidebands of the solitons are significantly enhanced. The experimental results confirm the theoretical predictions as shown in Fig. 3. From Fig. 11(b), we can see that the spectral width of the pulses is about 0.96 nm, and the autocorrelation trace has a full width at half maximum of 4.7 ps, corresponding to the pulse duration of about 3 ps. Then, the time-bandwidth product is 0.353, showing that it is $\text{sech}^2$-shaped pulses rather than Gaussian-shaped pulses. Obviously, this value is larger than 0.315 of bandwidth-limited $\text{sech}^2$-shaped pulses. It originates from the fact that the pulses attach some chirp after they are amplified by the EDF [Fig. 9(c)].

The experimental results show that, when the pump power is beyond 50 mW, the rectangular pulses with a nanosecond scale are observed. The pulse profiles are similar to the reports in Ref. [27]. In this case, the spectral sidebands disappear.

By using a material-based saturable absorber, such as the carbon nanotube and graphene [28], the conventional solitons with spectral sidebands are observed experimentally. They are similar to Fig. 11. Here, it is suggested that the theoretical findings are available to the mode lockers based on the saturable absorbers of the carbon nanotube and graphene.

## V. CONCLUSIONS

Based on the nonlinear polarization rotation technique and the intracavity filtering effect, we numerically and experimentally have investigated the soliton formation and evolution in passively-mode-locked lasers where pulses encounter ultralong anomalous-GVD fibers. Two balances, nonlinearity and anomalous-GVD balance and intracavity filtering and SAM balance, determine the soliton formation and evolution in the proposed lasers. Numerical simulations show that a higher-energy soliton breaks up into multiple lower-energy solitons with exactly the same physical properties. It is the mechanism of pulse splitting that manages the multisoliton formation in the proposed laser rather than the mechanism of soliton shaping from the linear waves. It is numerically found that the separation of neighboring solitons is variational in the temporal domain. The temporal and spectral characteristics of the solitons have large variations throughout the laser cavity (e.g., the pulse-breathing ratio in the SMF is more than 2), qualitatively distinct from the steady state of conventional solitons. The experimental observations confirm the theoretical predictions.

## ACKNOWLEDGMENTS

This work was supported by the National Natural Science Foundation of China under Grant No. 10874239 and No. 10604066. The author would especially like to thank Dong Mao and Xiaohui Li for help with the experiments.

[1] R. Weill, A. Bekker, V. Smulakovsky, B. Fischer, and O. Gat, Phys. Rev. A **83**, 043831 (2011).
[2] A. Komarov, H. Leblond, and F. Sanchez, Phys. Rev. E **72**, 025604(R) (2005).
[3] M. Salhi, F. Amrani, H. Leblond, and F. Sanchez, Phys. Rev. A **82**, 043834 (2010).
[4] B. G. Bale, S. Boscolo, J. N. Kutz, and S. K. Turitsyn, Phys. Rev. A **81**, 033828 (2010).
[5] V. L. Kalashnikov and A. Apolonski, Phys. Rev. A **79**, 043829 (2009).
[6] X. Liu, Phys. Rev. A **82**, 053808 (2010).
[7] E. Ding, E. Shlizerman, and J. N. Kutz, Phys. Rev. A **82**, 023823 (2010).
[8] S. Chouli and P. Grelu, Phys. Rev. A **81**, 063829 (2010).
[9] X. M. Liu, Opt. Express **17**, 22401 (2009); Phys. Rev. A **81**, 053819 (2010).
[10] D. Mao, X. M. Liu, L. R. Wang, X. H. Hu, and H. Lu, Laser Phys. Lett. **8**, 134 (2011).
[11] A. B. Grudinin, D. J. Richardson, and D. N. Payne, Electron. Lett. **28**, 67 (1992); L. R. Wang, X. M. Liu, Y. K. Gong, D. Mao, and X. H. Li, *ibid*. **46**, 436 (2010).
[12] F. X. Kärtner, J. Aus der Au, and U. Keller, IEEE J. Sel. Top. Quantum Electron. **4**, 159 (1998).
[13] F. W. Wise, A. Chong, and W. Renninger, Laser Photonics Rev. **2**, 58 (2008).
[14] O. E. Martinez, R. L. Fork, J. P. Gordon, Opt. Lett. **9**, 156 (1984); H. A. Haus, E. P. Ippen, and K. Tamura IEEE J. Quantum Electron **30**, 200 (1994).

[15] L. E. Nelson, D. J. Jones, K. Tamura, H. A. Haus, and E. P. Ippen, Appl. Phys. B **65**, 277 (1997).
[16] J. M. Soto-Crespo, M. Grapinet, P. Grelu, and N. Akhmediev, Phys. Rev. E **70**, 066612 (2004).
[17] W. Chang, J. M. Soto-Crespo, A. Ankiewicz, and N. Akhmediev, Phys. Rev. A **79**, 033840 (2009).
[18] D. Y. Tang, L. M. Zhao, B. Zhao, and A. Q. Liu, Phys. Rev. A **72**, 043816 (2005).
[19] X. Liu, Phys. Rev. A **81**, 023811 (2010); **82**, 063834 (2010).
[20] G. P. Agrawal, *Nonlinear Fiber Optics*, 4th ed. (Academic, Boston, 2007).
[21] G. P. Agrawal, IEEE Photonics Technol. Lett. **2**, 875 (1990).
[22] A. Cabasse, B. Ortaç, G. Martel, A. Hideur, and J. Limpert, Opt. Express **16**, 19322 (2008).
[23] G. Martel, C. Chédot, V. Réglier, A. Hideur, B. Ortaç, and P. Grelu, Opt. Lett. **32**, 343 (2007).
[24] X. M. Liu and B. Lee, IEEE Photonics Technol. Lett. **15**, 1549 (2003).
[25] J. P. Gordon, J. Opt. Soc. Am. B **9**, 91 (1992); S. M. J. Kelly, Electron. Lett. **28**, 806 (1992).
[26] X. Liu, L. Wang, D. Mao, and X. Li, J. Mod. Opt. **57**, 1635 (2010).
[27] W. Li, Q. Hao, M. Yan, and H. Zeng, Opt. Express **17**, 10113 (2009); L. M. Zhao, D. Y. Tang, T. H. Cheng, and C. Lu, Opt. Commun. **272**, 431 (2007).
[28] H. Zhang, Q. Bao, D. Tang, L. Zhao, and K. Loh, Appl. Phys. Lett. **95**, 141103 (2009); Z. Sun, D. Popa, T. Hasan, F. Torrisi, F. Wang, E. Kelleher, J. Travers, V. Nicolosi, and A. Ferrari, Nano Res. **3**, 653 (2010); S. Kivistö, T. Hakulinen, A. Kaskela, B. Aitchison, D. Brown, A. Nasibulin, E. Kauppinen, A. Härkönen, and O. Okhotnikov, Opt. Express **17**, 2358 (2009); F. Wang, A. Rozhin, V. Scardaci, Z. Sun, F. Hennrich, I. White, W. Milne, and A. Ferrari, Nat. Nanotechnol. **3**, 738 (2008).